J. Wind Eng. Ind. Aerodyn. 143 (2015) 42–49

Contents lists available at ScienceDirect

Journal of Wind Engineering and Industrial Aerodynamics

journal homepage: www.elsevier.com/locate/jweia

Aerodynamic forces on the roofs of low-, mid- and high-rise buildings subject to transient winds

Michael Jesson [a,*], Mark Sterling [a], Chris Letchford [b], Chris Baker [a]

[a] School of Civil Engineering, University of Birmingham, Birmingham, UK
[b] School of Civil and Environmental Engineering, Rensselaer Polytechnic Institute, NY, USA

ARTICLE INFO

Article history:
Received 13 October 2014
Received in revised form
30 March 2015
Accepted 24 April 2015
Available online 28 May 2015

Keywords:
Downbursts
Thunderstorms
Transient winds
Wind loading
Structures

ABSTRACT

Transient winds, such as thunderstorm downbursts, are the cause of design-load wind speeds in many countries. An understanding of the loading experienced by buildings during a downburst is therefore important to allow well designed and engineered buildings to be constructed. In contrast to boundary layer winds, the maximum wind speed in thunderstorm downbursts occurs as low as $z_m = 30$ m above the ground, within the range of heights of man-made structures, suggesting that the wind loading will be dependent on the building eaves height relative to z_m. In a novel set of experiments, the University of Birmingham Transient Wind Simulator (a 1 m diameter impinging jet with aperture control) has been used to simulate a downburst striking buildings of different heights, ranging from below to above z_m. Two forms of building have been used – a square-plan, flat-roofed structure, and a rectangular, portal-frame – at three angles (0°, 45° and 90°) relative to the radial wind direction. Pressure coefficients have been calculated (using eaves height velocity) over the roofs of these buildings, and are shown to be of greatest magnitude when the roof is above the region of maximum outflow velocity, with the exception of windward edges perpendicular to the flow, when they are generally greatest for the lowest building heights.

1. Introduction

Convection in thunderstorm cells can lead to the development of tornadoes or thunderstorm downbursts, i.e., transient wind events which have a short duration but which produce high wind speeds. These speeds are the building design wind speeds in many parts of the world (Chay and Letchford, 2002a).

Downbursts are formed when upward air currents in the convection region of a thunderstorm cool rapidly due to the evaporation of precipitation (Wakimoto and Bringi, 1988). The cooled air is denser than the surrounding air and falls to the ground, with a ring vortex forming (see Vermeire et al (2011) for details). This vortex is carried outwards with the radial outflow which forms when the downdraft impinges on the ground (Fujita, 1981), leading to high wind speeds in the near ground region. In contrast to the monotonically increasing vertical profiles of velocity in ABL flow, the maximum velocity in a downburst outflow occurs at a height $z_m = 30$–100 m above the ground (Fujita and Wakimoto, 1981; Hjelmfelt, 1988).

The most intense downbursts, termed microbursts by Fujita (1981), have a diameter of only ~1000 m and a lifetime of ~5 min (Fujita, 1981; Holmes et al. 2008) and consequently are difficult to measure at full-scale. Despite efforts such as the NIMROD and JAWS projects (Fujita, 1981), and (more recently) the Thunderstorm Outflow Experiment (Gast and Schroeder, 2003; Holmes et al. 2008), only a small number of full-scale downbursts have been measured, providing a limited data set to aid the understanding of these events. When considering wind loading on structures, the unpredictability of where and when a downburst will strike makes it very difficult to obtain full-scale pressure measurements over a structure – the chances of a single, instrumented building being subject to a downburst are extremely small. Lombardo (2009) has, however, successfully identified a small number of downburst events from historical velocity data recorded at the Texas Tech University Wind Engineering Field Research Laboratory (WERFL), and examined the corresponding pressure data from tappings over the WERFL building (a 9 m × 14 m × 4 m tall, rectangular plan building).

Notwithstanding Lombardo's success in measuring data at full-scale, the physical simulation of downbursts in engineering laboratories is essential in order to understand their impact on structures of different types and proportions. A variety of methods have been used to physically simulate downbursts: very small-scale density driven flows (e.g. Lundgren et al. 1992); slot jets (e.g. Butler

* Corresponding author at: School of Civil Engineering, University of Birmingham, Edgbaston, Birmingham, B15 2TT, UK. Tel.: +44 121 414 5065.
E-mail address: m.a.jesson@bham.ac.uk (M. Jesson).

http://dx.doi.org/10.1016/j.jweia.2015.04.020

and Kareem, 2007; Lin et al. 2007); multi-fan wind tunnels (e.g. Butler et al. 2010); steady impinging jets (e.g. Chay and Letchford, 2002a, 2002b; Choi, 2004; Wood et al. 2001; Zhang et al. 2014, 2013 and pulsed impinging jets (e.g. Haines et al. 2013; Jesson et al. 2015; Mason, 2003; Mason et al. 2009a; McConville et al. 2009). As has been discussed by Vermeire et al. (2011), who compared numerical simulations of impinging jets and cooling source downbursts, fan-driven impinging jets do not have the same forcing mechanism as a full-scale downburst and so do not provide a full simulation of a downburst despite the creation of a ring vortex. Having examined the data presented by Vermeire et al. (2011), the authors believe that, at the time and location of maximum radial velocity, the pulsed impinging jet facility used by Jesson et al. (2015) is a reasonable approximation to the flow field of a downburst. As such, the simulations performed at this facility, the University of Birmingham Transient Wind Simulator (UoB-TWS), constitute a partial simulation which may be used to investigate the transient pressure field on a structure as the ring vortex passes over it. The UoB-TWS was used for the work presented in this paper, and it is described in Section 2.1.

The distinction between low- and high-rise buildings is particularly important in the context of downbursts, due to the closeness of z_m to the ground. In the context of atmospheric boundary layer (ABL) winds, low-rise buildings have been defined as those with width greater than twice the height, h, and $h < 30$ m (Uematsu and Isyumov, 1999). When discussing downbursts, a natural definition of low- and high-rise is that the eaves height of a low-rise structure is below z_m while that of a high-rise structure is above; in the context of this study, this definition is consistent with that for ABL flow. Although a number of the aforementioned studies have measured the pressure field over building models (e.g. Chay and Letchford, 2002a, 2002b; Jesson et al. 2015; Mason et al. 2009a; Sengupta et al. 2008; Sengupta and Sarkar, 2008), the small length scale ($\sim$1:1600 in the case of Jesson et al. 2015) and value of z_m of these simulations means that these buildings are high-rise structures under this definition. The pressure field on the walls of prismatic, low-rise buildings subject to a simulated transient gust front has been measured by Butler et al. (2010), using a multi-fan, variable speed wind tunnel to simulate a rapid increase in velocity. No pressure measurements were made on the model roofs by Butler et al., and their work may be limited by not simulating the vortex-driven nature of the downburst flow field-turbulence intensity is known to affect flow separation around bluff bodies (Jensen, cited by Melbourne (1993), Holmes (2001)) and hence not recreating the vorticity field of a downburst may affect the pressures measured. The work described in this paper extends the work of Jesson et al. (2015) to a range of building heights, from low- to high-rise, allowing the effect of building height relative to z_m to be determined.

This paper presents the findings of a research project aimed at quantifying the pressure field on low-, mid- and high-rise structures in transient, downburst winds, and how the field varies with building height. It extends the work of Jesson et al. (2015) by varying the height of the model buildings subjected to a simulated downburst-type wind. In doing so, the variation of the pressure field due to the building eaves height relative to z_m is measured, and the pressure field due to a downburst elucidated for both low- and high-rise buildings. Following this introduction, the UoB-TWS, the experimental facility used to gather the data presented in this paper, is described in Section 2. The pressure and force coefficients measured over building models with a range of heights spanning low- to high-rise, subject to a simulated thunderstorm downburst, are presented and discussed in Section 3. Section 4 summarises the important conclusions drawn from the work.

2. Experimental setup

2.1. University of Birmingham Transient Wind Simulator (UoB-TWS) facility

The UoB-TWS, originally developed by McConville et al. (2009), is an impinging jet facility with a vertical, circular, downward jet of diameter $D = 1$ m. It has subsequently been improved and in its current incarnation uses nine 0.85 m^2 cross-section axial flow fans to direct air into a settling chamber which, in turn, feeds a circular nozzle, the exit of which is controlled by a set of eight flaps. The opening of these flaps is controlled by the same computer and software which controls the fan speed in order to make the experimental runs as repeatable as possible. In this way, rapidly accelerating downward flow is created which causes the formation of an entrainment vortex at the interface between the jet and the surrounding air. When the jet impinges on the ground plane, this ring vortex travels with the outflow. The jet velocity (V_j), measured immediately below the nozzle exit, has a mean value of 13.1 m s^{-1} (with negligible variation over the central 90% of the diameter (McConville, 2008)), and a turbulence intensity of 13%. In order to permit instruments to be installed as closely as possible to the downburst (to, for example, minimise tube lengths to pressure tappings), the jet impinges onto a raised ground plane (Fig. 1).

More detail of the UoB-TWS may be found in McConville et al. (2009) and Jesson et al. (2015).

2.2. Simulated flow field

Previous work has shown that the scales of the physical simulations may be estimated as 1:1600, 1:2.6 and 1:600 for length, velocity and time, respectively. Using these scales gives a good match to full-scale data (Fig. 2 and Jesson et al (2015)), with the simulation data showing the peak velocity and the initial rapid acceleration of a full-scale event; the full-scale data is from the Andrews Air Force Base (AAFB) event, described by Fujita (1985). The velocity measurements were made at a range of radial distances, r, from the centre of the downdraught, with $r/D = 1.0$, 1.25, 1.5, 1.75, 2.0 and 2.5, at 10 mm (16 m full-scale) vertical increments spanning 0.01–0.25 m (16–400 m full-scale) from the ground plane (Jesson et al. 2015). A ten-run, ensemble-mean approach was used (following McConville et al (2009)) to allow generic features of downbursts to be examined in isolation from the run-to-run variation which is a feature of both full-scale downbursts (for example, Choi, 2004; Hjelmfelt, 1988; Lombardo, 2009) and UoB-TWS runs. A fifty-point moving average

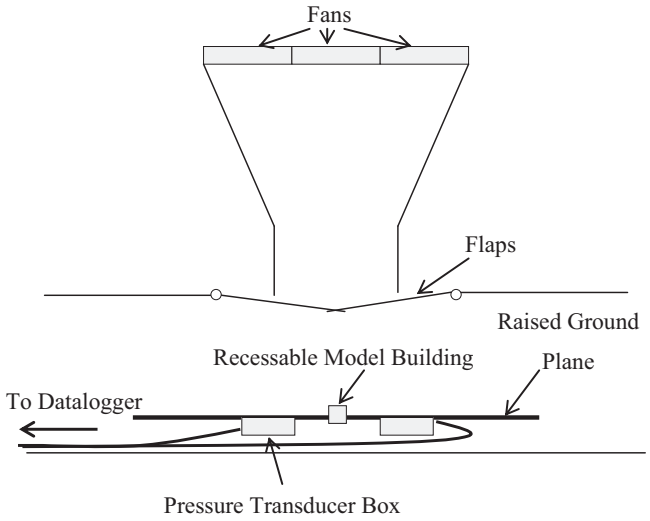

Fig. 1. A schematic of the UoB-TWS facility (Jesson et al. 2015).

was applied to the velocity measurements, giving values equivalent to full-scale gusts of approximately 3 s duration (based on the sampling rate of 10 kHz and time scale), and all values presented are these gust values. The peak maximum radial velocity (i.e. the temporal maximum at the location with the highest wind speed, $U=19.4\ \mathrm{m\ s^{-1}}$) was found to occur at a radial distance $r/D=1.5$ from the centre of the downburst (Jesson et al. 2015), with the vertical profile of U showing the typical "nose" of a downburst outflow wind (Fig. 3), and a region of maximum U centred at $z=20$ mm. The envelope of run velocities at each height (the maximum and minimum values from all runs at the time of the ensemble maximum), gives an indication of the run-to-run variation (Fig. 3). As found by McConville (2008), this variation is large (approximately $\pm 25\%$ maximum), but the downburst profile is retained; further, Jesson et al. (2015) showed that force coefficients calculated from the ensemble approach are comparable to those from a single run "maximum".

Flow visualisation on the UoB-TWS has been performed by McConville et al (2009) and Haines (2015), which has shown the evolution of the ring vortex. It was not possible to use the flap mechanism for this work, and so only a rough estimate of the vortex size for a full simulation can be made. Results show that the vortex core is above the height of the building used in the current work, consistent with the numerical simulations of Mason et al (2009b).

Radial turbulence intensity has been calculated for each of the 10 experimental runs at each height using the wavelet method described by Jesson et al. (2015), itself similar to the method of Wang and Kareem (2004). From these runs, an ensemble-mean TI time-series was calculated and a 50-point moving average applied, as for the velocity measurements. The maximum value from each smoothed, ensemble-mean time-series (each for a different height, z) is shown in Fig. 3. Also included in this figure is an ABL vertical profile of TI, calculated using the relationship given by Holmes (2001):

$$TI = \frac{1}{\ln\left(\frac{z}{z_0}\right)} \tag{1}$$

where z_0 is a roughness length for the terrain, set to $z_0=0.005$ m for the smooth floor of the UoB-TWS. Close to the ground plane, at $z/z_m=0.5$, the TI is approximately double the ABL value. Between $1.0 \le z/z_m \le 2.5$ the downburst and ABL TIs are within 0.5% of each other (though clearly this is dependent on the choice of z_0), and above this region it falls to approximately 60% of the ABL value. It is cautiously hypothesised that the high value near the ground is due to a combination of a thin, low-speed sub-layer near the surface (due to the no-slip condition) and the high-speed vortex flow above it. Together, these lead to a region of high shear and generation of small scale vorticity at the boundary between the fast and slow regions of flow. Phase-plots of the velocity data (not shown) point to the existence of a small, secondary vortex leading the main ring vortex, as previously indicated by numerical simulation (Kim and Hangan, 2007; Mason et al. 2009b). The interaction of the two vortices may be the cause of the elevated TI between $1.0 \le z/z_m \le 2.5$.

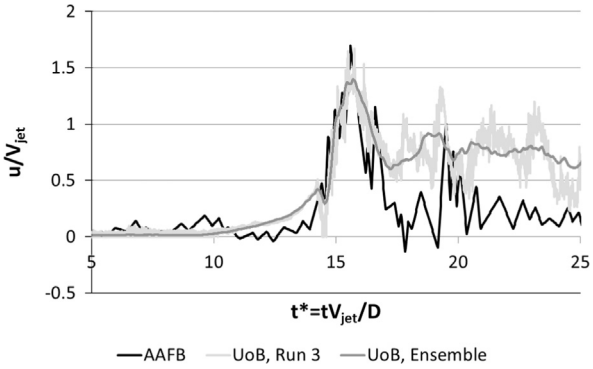

Fig. 2. Time-series of radial velocity from a full-scale downburst and UoB physical simulations (ensemble mean and an example of a single run).

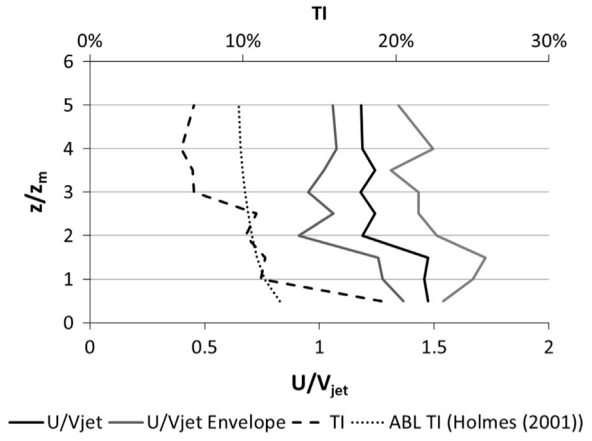

Fig. 3. Vertical profiles of ensemble-mean radial velocity (lower horizontal axis) and radial turbulence intensity (upper horizontal axis) at $r/D=1.5$.

2.3. Building models and pressure measurement

The pressure-tapped building models used for this research are illustrated and summarised in Fig. 4 and Table 1, and described fully in Jesson et al. (2015). Model height is expressed in terms of a Normalised Eaves Height (NEH), the ratio of building eaves height, h, to the height at which the peak maximum radial velocity occurred, z_m (i.e. $\mathrm{NEH}=h/z_m$). This allows simple identification of whether a building is low-, mid- or high-rise in respect to a downburst.

The pressure field over the buildings was measured using a bespoke, 64-channel digital pressure measurement system (DPMS) at a rate of 500 Hz. Differential pressures (relative to the atmospheric pressure in the laboratory at a position remote from the UoB-TWS, and referred to as p_{atm}) were recorded. The pressure time-series were smoothed using a three-point moving average; this is equivalent to full-scale gusts of duration approximately 3 s, using the assumed scales.

All pressure measurements were made at a radial distance $r/D=1.5$. The building models were mounted on a turntable to allow the effects of different yaw angles (angle of incidence of the wind onto the model, see Fig. 4) to be examined. The turntable was also equipped with a mechanism to recess the building into the ground plane, allowing changes in the pressure field with building height to be examined, in particular the effect of moving through the vertical position of maximum radial velocity, $z_m=20$ mm. A range of eaves heights was used for each building: 5 mm, 10 mm, 20 mm, 30 mm, 40 mm and 60 mm for the recessed cube (RC), and 0 mm, 5 mm, 10 mm, 20 mm, 30 mm and 42 mm for the portal-framed building; the last is full height in each case.

3. Aerodynamic pressure coefficients

The transient nature of downburst flows means that both U and the static pressure are time-varying quantities. Consequently, decisions must be made when calculating typical wind loading parameters as to which values to use. Pressure coefficients (C_p) are typically defined as:

$$C_p = \frac{p - p_{ref}}{\frac{1}{2}\rho V^2} \tag{2}$$

where p is the absolute pressure, p_{ref} is a reference pressure, ρ the air density and V a velocity used to calculate a reference dynamic

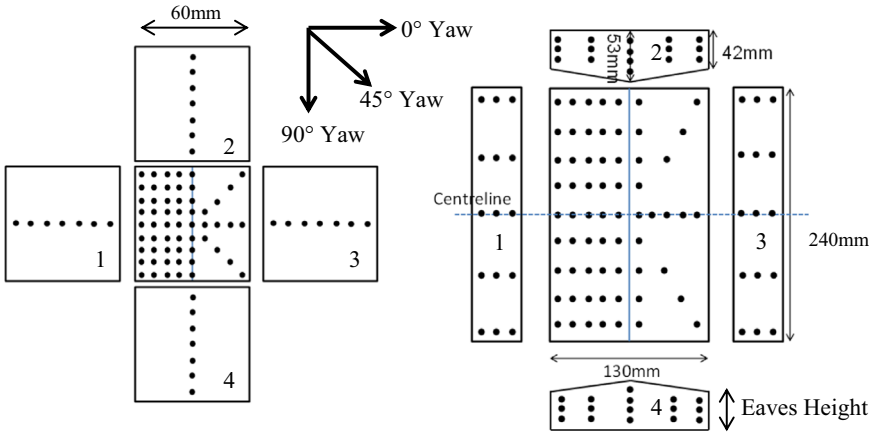

Fig. 4. The model building pressure tapping positions and face numbering (not to scale) (a) 60 mm cube; (b) portal frame.

Table 1
Model building dimensions, including when recessed.

Model	Height (mm)		NEH	Width (mm)	Length (mm)	Roof pitch (°)
Portal	42 (eaves)	53 (ridge)	2.10	130	240	10
	30	41	1.50			
	20	31	1.00			
	10	21	0.50			
	5	16	0.25			
Cube	60		3.00	60	60	0
	40		2.00			
	30		1.50			
	20		1.00			
	10		0.50			
	5		0.25			

pressure for normalisation. Assuming negligible openings in the building, the internal pressure will remain approximately constant over a short duration transient wind event, at the atmospheric value before the downburst, p_{atm}. The differential pressures $(p - p_{atm})$ measured by the DPMS may therefore be used directly in the downburst case. In the case of (stationary) ABL flow, the eaves height wind-speed (or mean roof height wind-speed for portal buildings) is typically used as V. It was postulated by Jesson et al. (2015) that the peak maximum wind speed is a better choice for V when comparing pressure fields with buildings of different heights subject to downbursts due to it representing the maximum wind speed on a windward face; however, as the current paper concerns roof pressures alone, the convention of using the eaves height wind-speed is used herein. Velocity data were not available for NEH=0.25 (h=5 mm), and so the eaves height velocity for this building height has been extrapolated from the measured values and the vertical distribution of radial velocity for a downburst given by Hjelmfelt (1988). While some design codes specify that h is the mean height of the roof, the US code allows h to be eaves height for roofs with pitch up to and including 10° (ASCE, 2010), the pitch of the portal-framed model, and this is followed herein.

Positions on the surface of the building are referenced using building co-ordinates, as defined in Fig. 5.

Relevant figures of results are included in this paper, while animations showing the pressure field contours over the entire roof are available, for a selection of the cases discussed, as supplementary content to the online article.

3.1. Recessed 60 mm cube (RC) – 0° yaw

The distribution of minimum pressure coefficient (maximum suction) along the roof centreline shows high leading edge suctions all NEHs, with $-0.9 \geq C_p \geq -1.2$ (Fig. 6; for convenience, insets to figures indicate building height with respect to the vertical velocity profile, and yaw angle). When along wind position, x, is scaled by the building length, X, the distributions appear to be dependent on NEH (Fig. 6a). Using an alternative normalisation, by building height, h, leads to a collapse of these distributions (Fig. 6b), with the possible exception of NEH=2.00. This case, the lowest in which the eaves height is above the region of maximum velocity, shows the greatest suctions, and appears to reach a limiting suction greater than the other cases (though the lack of data for greater x/h makes this somewhat speculative). The greater magnitude of the pressure coefficient for this case may be due to the high velocity region being sufficiently close to the top of the model to be significantly affecting the flow over the model, while the eaves height velocity used for the pressure coefficient calculation is relatively small.

Comparison with the work of Mason (2009a) is complicated by the need to scale their results (which used the jet velocity in the pressure coefficient calculation), as there is no clear z_m in their data. Estimating their NEH as 2.00, the two data sets are consistent bearing in mind the associated uncertainties (Fig. 7).

Fig. 8 shows the minimum pressure coefficients which occur along the windward roof edge of the RC during a simulated downburst, from which it is clear that asymmetry of the distribution occurs. With the building having been positioned as precisely as possible, it is thought that the asymmetry may be due to unavoidable irregularities in the ground plane, asymmetry of the jet outflow or high sensitivity to slight misalignment of the model building. A programme of CFD work is underway which may shed more light on this issue. It is evident that the distribution is different for the lowest eaves height (NEH=0.25), with minimum pressure either side of the centreline, a slight reduction in the centre and significant ($>30\%$) reduction in magnitude close to the outer edges of the roof. This difference may be due to the sub-layer adjacent to the ground plane (discussed in Section 1) enveloping the sides of the building at this eaves height, preventing flow separation and interacting with the flow at the edges of the roof. From the other NEHs, the pressure coefficients are lowest for NEH=2.00, as seen for the centreline values, and the same reasoning for this applies.

3.2. Recessed 60 mm cube (RC) - 45° yaw

For a yaw angle of 45° it has been shown that, for the full height cube (NEH=3.0), minimum pressure coefficients occur along the windward edges due to the formation of delta wing vortices (Jesson et al. 2015). Data are presented here for one of these edges (Fig. 9). For NEH=0.25 there is no clear evidence for the formation

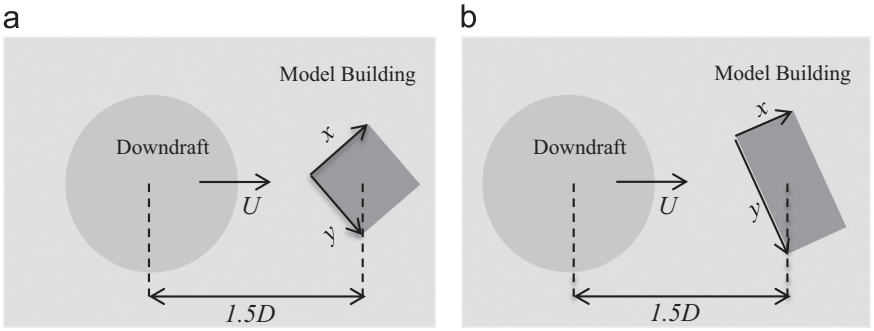

Fig. 5. Plan view schematic of the building axes for the recessed (a) cube and (b) portal buildings. For 0° yaw, U is parallel to the x-axis. The z-axis is out of the page.

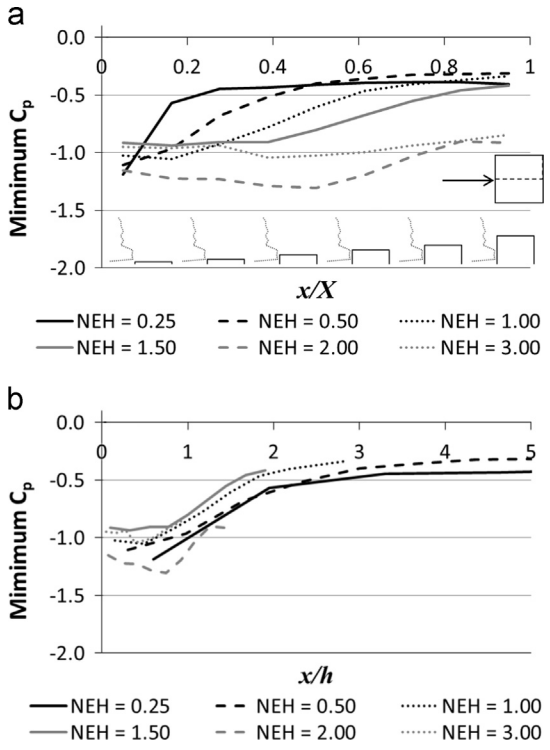

Fig. 6. Minimum pressure coefficient at each centreline tapping of a recessed 60 mm cube at 0° yaw at a number of eaves heights. Position along the centreline, x, is normalised by (a) building length in the x-direction, X, (b) building height, h.

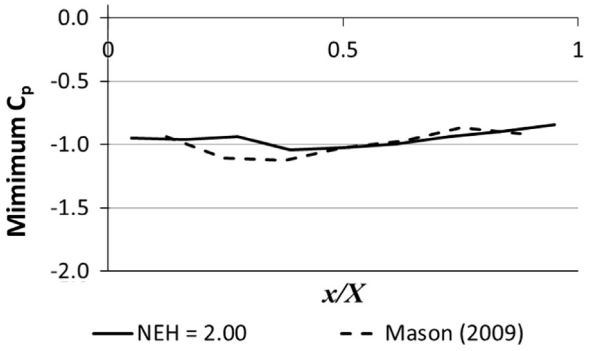

Fig. 7. Minimum pressure coefficient at each centreline tapping of a recessed 60 mm cube at 0° yaw at NEH=2.00, and the approximately equivalent data of Mason et al. (2009a). Position along the centreline, x, is normalised by building length in the x-direction, X.

of delta wing vortices, and the distribution is qualitatively as for the 0° yaw case. Again, this may be caused by a sub-layer forming close to the ground plane, preventing the normal flow interactions

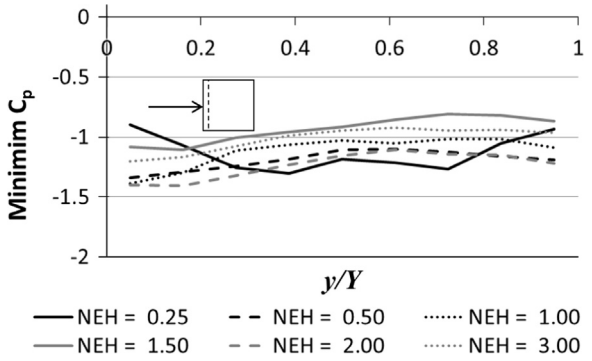

Fig. 8. Minimum pressure coefficients along the windward roof edge of a recessed 60 mm cube at a number of eaves heights at 0° yaw angle.

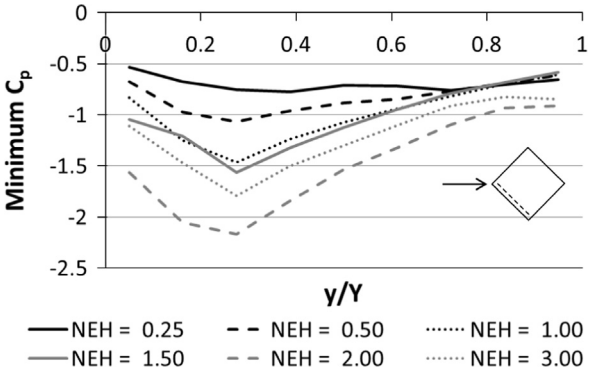

Fig. 9. Minimum pressure coefficient at each windward edge tapping of a recessed 60 mm cube at 45° yaw at a number of eaves heights. Position normalised by face length, Y.

with the building edges. For NEH ≥ 0.50, these distributions are consistent with the formation of delta wing vortices which expand (and weaken in intensity) with distance along the roof edge. As with the 0° yaw, the minimum pressure coefficients ($C_p = -2.2$) occur for an NEH of 2.00. For ABL flow, Gerhardt and Kramer (1992) suggest that for $h/B \leq 0.2$ (NEH ≤ 0.6 in this work) the minimum pressure should be constant for all NEH. Therefore the variation seen (certainly for low NEH) is due to the vertical velocity profile and the change in the position of the roof relative to z_m, rather than the changing geometry.

3.3. Recessed 240 mm ridge, 130 mm wide, portal building – 0° yaw

The centreline ($y/Y = 0.5$) pressure coefficient distribution is height dependent for the portal building (Fig. 10). Unlike the RC results, for a 0° yaw angle (radial wind perpendicular to the ridge), for NEH = 0.25 there is no low pressure at the leading edge, with

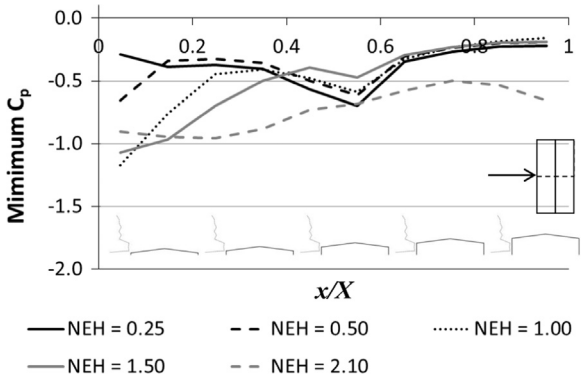

Fig. 10. Minimum pressure coefficient at each centreline tapping of a recessed 240 mm ridge length, 130 mm wide, portal-framed building at 0° yaw at a number of eaves heights. Position along the centreline, *x*, is normalised by building length in the *x*-direction, *X*.

the minimum C_p (≈ -0.7) at the leeward edge of the ridge line, with a slightly higher pressure ($C_p \approx -0.5$) on the windward edge of the ridge. This implies that, despite being relatively small ($\sim 10°$) the roof pitch is preventing flow separation at the leading edge at the low radial velocities seen near the ground plane. This is discussed further below. The ridge line, being 11 mm higher than the eaves (at a normalised ridge height (NRH) of 0.8), lies in higher speed flow and so separation occurs. The ridge line suction is about 60% of the values seen for the RC leading edge, probably due the smaller change in angle between the relevant building faces (90° between the RC wall and roof, 20° between the two roof pitches of the portal building). At NEH=0.5 leading edge flow separation becomes apparent and is of the same magnitude as that seen at the ridge line. As NEH increases to 1.0, the windward edge pressure decreases to $C_p \approx -1.2$, the maximum suction seen for this configuration, and equal to the maximum seen for the RC. Ridge line suction is slightly reduced in magnitude from the NEH=0.25 value, being $C_p \approx -0.6$. For the full-height building (NEH=2.1; NRH=2.7), the high ridge line suction is no longer evident as a local minimum pressure coefficient, due to the ridge being well within the low velocity region, but the pressure coefficients are at a minimum over the entire centreline except for the leading edge. The NEH corresponding to the greatest suctions therefore matches that seen for the recessed cube.

With a steady impinging jet, a boundary layer develops with distance from the stagnation region (Xu and Hangan, 2008), and similarly a viscous sub-layer may form adjacent to the ground plane in the transient flow, lifting the ring vortex which then impacts the model on the pitched roof rather than the windward face for NEH=0.25. The different flow regimes hitting the building above and below the eaves, in conjunction with the roof pitch, may then prevent flow separation from occurring. As NEH increases, the eaves fall within the vortex and separation again occurs.

When plotting distance normalised by building height (not shown), a collapse of the distributions occurs for the region upwind of the ridge, similar to that seen for the RC, except for NEH=0.25. The presence of the ridge, and the low pressure downwind of it, leads to a breakdown of this relationship further along the centreline due to the change in the normalised position of the ridge with NEH. When assessing cladding loads for a ridged building, therefore, a different scaling system is required for the leading edge region and the region around the ridge(s).

The reduction in magnitude of the pressure at the windward roof edge for low eaves heights occurs at all positions along the windward edge (not shown), while for NEH > 0.50 the magnitudes are as for the recessed cube.

3.4. Recessed 240 mm ridge, 130 mm wide, portal building – 45° yaw

As discussed previously, with a 45° yaw angle the windward edge C_p distribution for the RC (Fig. 9) shows the formation of delta wing vortices for all but the lowest NEH. Fig. 11 shows equivalent time-series for the portal building, but includes data for edges bordering both Face 1 and Face 2 (as defined in Fig. 4), corresponding to the lines $x/X \approx 0$ ("Edge 1") and $y/Y \approx 0$ ("Edge 2") respectively, since the profile of these faces is different. The same results are seen for the portal building as for the RC, with clear regions of high suction in the first quarter of the windward edges. Ridge line suction is also seen, as for the centreline of portal framed building at 0° yaw (Fig. 10), for NEH < 1.00 (this ridge suction may occur at greater NEH, but the suction due to the delta wing vortex, and the lack of pressure tappings after the ridge on Edge 2, mean this cannot be verified). In contrast to the 0° yaw centreline case, greatest suction occurs for NEH=2.10, rather than 1.00, with $C_p \approx -2.3$ at $y/Y=0.14$ and $C_p \approx -2.5$ at $x/X=0.15$. It should be noted that although these normalised locations are approximately equal, in absolute terms they are 34 mm and 20 mm, respectively. It would therefore appear that the pitch along Edge 2 is affecting the formation of the delta vortex, moving the position of maximum vorticity closer to the windward corner. These locations are also independent of NEH (for NEH sufficiently high for the delta wing vortices to form), and so normalisation by *h* will not give NEH independent results.

3.5. Recessed 240 mm ridge, 130 mm wide, portal building – 90° yaw

With the portal building at a yaw angle of 90° (Face 2 perpendicular to the radial outflow), the "centreline" is a small distance from the ridge line (see Fig. 4) due to the position of the tappings, but the terminology is retained for convenience. C_p time-series and minima along the centreline (not shown) generally match those for the RC once the differences in building length and tapping height (due to the roof pitch) have been taken into account. There is more spread at the leading edge, with C_p ranging from -0.6 to -1.2, but over the remainder of the centreline the highest suction is seen for NEH=2.10. The time-series are not presented or discussed further here as the differences may be illustrated by the windward edge minima values discussed below.

Minimum pressure coefficients along the windward edge with 90° yaw (Fig. 12) have more in common with the 0° yaw RC data than the 0° yaw portal data. This is to be expected as with Face 2 perpendicular

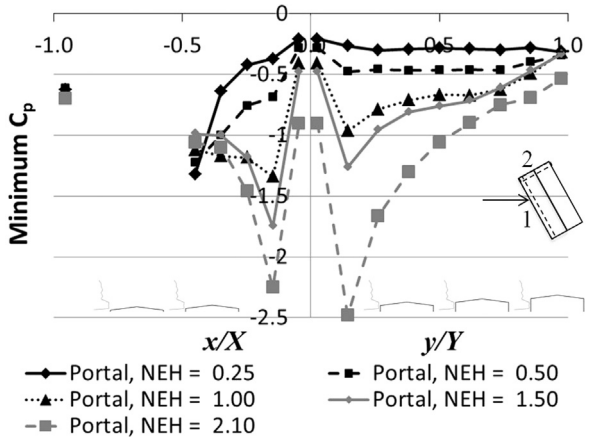

Fig. 11. Minimum pressure coefficients along the windward roof edge of a recessed 240 mm ridge, 130 mm wide portal building at a number of eaves heights at 45° yaw angle. Negative distances refer to Edge 2, with 0 being the Edge 1/Edge 2 (windward) corner – see inset for edge numbering. Interpolated values on Edge 2 are not included. Missing data are due to there being no pressure tappings in that region of the roof (see Fig. 4).

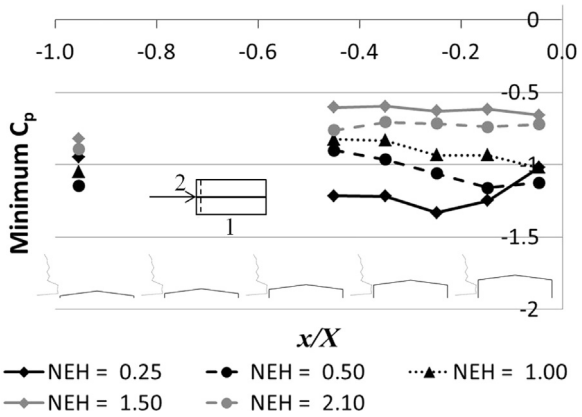

Fig. 12. Minimum pressure coefficients along the windward roof edge of a recessed 240 mm ridge, 130 mm wide portal building at a number of eaves heights at 90° yaw angle. Negative distances refer to Face 2, with 0 being the Face 1/Face 2 corner. Missing data are due to there being no pressure tappings in that region of the roof (see Fig. 4).

to the radial outflow there is a transition from a vertical to a radially horizontal building edge, rather than from a vertical to a 10° pitched roof as in the 0° yaw portal case. The reduction in magnitude at the end of the face for NEH=0.25 is evident and of a similar magnitude to that seen for the RC. Pressure coefficient magnitudes are smaller for other NEHs, however. For NEH=2.10 this is due to the ridge height being above the region of maximum velocity, but it also appears that the roof shape (angled across the radial flow direction) is preventing flow separation developing as for a horizontal roof edge.

4. Conclusions

In contrast to ABL winds, the maximum wind speed in thunderstorm downbursts occurs as low as z_m=30 m above the ground. Clearly, z_m lies above the eaves high of low-rise buildings but below that of high-rise buildings, suggesting that there may be a difference in the roof wind loading due to a downburst in each case. In a novel set of experiments, the effect of building height, h, on pressure coefficients on the roofs of model buildings in a simulated downburst has been investigated. Two models were used, a cube and a portal-framed building, which were recessed into a fixed ground plane to give square-plan building models ("recessed cube") and portal building models of varying eaves heights. The eaves heights of these models ranged from below z_m ("low-rise") to above z_m ("high-rise"), with eaves heights approximately equal to z_m defined as "mid-rise". Pressure coefficients have been measured over the roofs of these building models as they have been subject to a transient, downburst-type flow.

As with ABL flow, high suction regions form at upwind roof edges when the radial outflow of the downburst is perpendicular to a face of the building. Even though the downburst event is short-lived, there is evidence to suggest that delta wing type vortices occur when the wind strikes the building at an oblique angle. Thus, relatively high suction regions tend to occur a quarter of the way along the upwind edges, albeit for short periods of time, for cornering winds. This observed behaviour is of considerable importance in building design.

The scaling of downburst type winds is fraught with difficulties and no universal approach currently exists. However, it is interesting to note that for flat-roofed structures, scaling the along-wind position by building height leads to a collapse of the along-wind distribution of pressure coefficient. This may provide a means of simplification when devising design methods for such buildings. Unfortunately, this relationship breaks down for more complex situations, e.g., oblique winds and portal framed buildings (for which the ridge line causes a second high suction region). For winds perpendicular to a building face, pressure coefficients generally attain their maximum magnitudes for the lowest building heights, although this leading edge suction is not seen for the lowest portal framed building. Further investigation is required to establish the reason for this. In all other cases, magnitudes are greatest when the eaves height is just above z_m, and then decrease with height above this point. It is clear from these results that building design for downburst-type winds will require different considerations depending on building height relative to z_m.

Future work based on the experimental data will include the calculation of force coefficients, allowing comparison between the values derived from current design codes and those seen in a physical simulation of a downburst-type wind.

Acknowledgements

This research has been made possible through the support of the Engineering and Physical Sciences Research Council through Grant number EP/J008281/1, for which the authors would like to express their gratitude. Thanks must also go to Mike Vanderstam for his assistance in building and maintaining the transient wind simulator.

References

American Society of Civil Engineers (ASCE), 2010. Minimum design loads for buildings and other structures (ASCE/SEI 7–10). American Society of Civil Engineers/Structural Engineering Institute.

Butler, K., Cao, S., Kareem, A., Tamura, Y., Ozono, S., 2010. Surface pressure and wind load characteristics on prisms immersed in a simulated transient gust front flow field. J. Wind Eng. Ind. Aerodyn. 98, 299–316.

Butler, K., Kareem, A., 2007. Physical and numerical modeling of downburst generated gust fronts. In: Proceedings of the 12th International Conference on Wind Engineering, Cairns, Australia, pp. 791–798.

Chay, M.T., Letchford, C.W., 2002a. Pressure distributions on a cube in a simulated thunderstorm downburst—Part A: stationary downburst observations. J. Wind Eng. Ind. Aerodyn. 90, 711–732.

Chay, M.T., Letchford, C.W., 2002b. Pressure distributions on a cube in a simulated thunderstorm downburst—Part B: moving downburst observations. J. Wind Eng. Ind. Aerodyn. 90, 733–753.

Choi, E.C.C., 2004. Field measurement and experimental study of wind speed profile during thunderstorms. J. Wind Eng. Ind. Aerodyn. 92, 275–290.

Fujita, T.T., 1981. Tornadoes and downbursts in the context of generalized planetary scales. J. Atmos. Sci. 38, 1511–1534.

Fujita, T.T., 1985. The Downburst: Microburst and Macroburst. University of Chicago Press, Chicago, Illinois.

Fujita, T.T., Wakimoto, R.M., 1981. Five scales of airflow associated with a series of downbursts on 16 July 1980. Mon. Weather Rev. 109, 1439–1456.

Gast, K.D., Schroeder, J.L., 2003. Supercell rear-flank downdraft as sampled in the 2002 thunderstorm outflow experiment. In: Proceedings of the 11th International Conference on Wind Engineering. ICWEIA, pp. 2233–2240.

Gerhardt, H.J., Kramer, C., 1992. Effect of building geometry on roof windloading. J. Wind Eng. Ind. Aerodyn. 43, 1765–1773.

Haines, M., Sterling, M., Quinn, A., 2013. Interference effects around two model high rise buildings in a simulated non-synoptic event. In: Proceedings of the European-African Conference on Wind Engineering.

Haines, M.R., 2015. The simulation of non-synoptic effects and their implications for engineering structures. School of Civil Engineering, University of Birmingham UK, Birmingham.

Hjelmfelt, M.R., 1988. Structure and life cycle of microburst outflows observed in Colorado. J. Appl. Meteorol. 27, 900–927.

Holmes, John D. Wind Loading of Structures, Spon Press, 2001, Print ISBN: 978-0-419-24610-7 eBook ISBN: 978-0-203-30164-7.

Holmes, J.D., Hangan, H.M., Schroeder, J.L., Letchford, C.W., Orwig, K.D., 2008. A forensic study of the Lubbock-Reese downdraft of 2002. Wind Struct. 11, 137–152.

Jesson, M., Sterling, M., Letchford, C., Haines, M., 2015. Aerodynamic forces on generic buildings subject to transient, downburst-type winds. J. Wind Eng. Ind. Aerodyn. 137, 58–68.

Kim, J., Hangan, H., 2007. Numerical simulations of impinging jets with application to downbursts. J. Wind Eng. Ind. Aerodyn. 95, 279–298.

Lin, W.E., Orf, L.G., Savory, E., Novacco, C., 2007. Proposed large-scale modelling of the transient features of a downburst outflow. Wind Struct. 10, 315–346.

Lombardo, F.T., 2009. Analysis and interpretation of thunderstorm wind flow and its effects on a bluff body. Texas Tech University.

Lundgren, T.S., Yao, J., Masour, N.N., 1992. Microburst modelling and scaling. J. Fluid Mech. 239, 461–488.
Mason, M.S., 2003. Pulsed jet simulation of thunderstorm downbursts. Civil Engineering, Texas Tech University.
Mason, M.S., James, D.L., Letchford, C.W., 2009a. Wind pressure measurements on a cube subjected to pulsed impinging jet flow. Wind Struct. 12, 77–88.
Mason, M.S., Wood, G.S., Fletcher, D.F., 2009b. Numerical simulation of downburst winds. J. Wind Eng. Ind. Aerodyn. 97, 523–539.
McConville, A.C., 2008. The physical simulation of thunderstorm downbursts. School of Civil Engineering, University of Birmingham Birmingham, UK.
McConville, A.C., Sterling, M., Baker, C.J., 2009. The physical simulation of thunderstorm downbursts using an impinging jet. Wind Struct. 12, 133–149.
Melbourne, W.H., 1993. Turbulence and the leading edge phenomenon. J. Wind Eng. Ind. Aerodyn. 49, 45–63.
Sengupta, A., Haan, F.L., Sarkar, P.P., Balaramudu, V., 2008. Transient loads on buildings in microburst and tornado winds. J. Wind Eng. Ind. Aerodyn. 96, 2173–2187.
Sengupta, A., Sarkar, P.P., 2008. Experimental measurement and numerical simulation of an impinging jet with application to thunderstorm microburst winds. J. Wind Eng. Ind. Aerodyn. 96, 345–365.
Uematsu, Y., Isyumov, N., 1999. Wind pressures acting on low-rise buildings. J. Wind Eng. Ind. Aerodyn. 82, 1–25.
Vermeire, B.C., Orf, L.G., Savory, E., 2011. Improved modelling of downburst outflows for wind engineering applications using a cooling source approach. J. Wind Eng. Ind. Aerodyn. 99, 801–814.
Wakimoto, R.M., Bringi, V.N., 1988. Dual-polarization observations of microbursts associated with intense convection: the 20 July storm during the MIST project. Mon. Weather Rev. 116, 1521–1539.
Wang, L., Kareem, A., 2004. Modeling of non-stationary winds in gust-fronts. In: Proceedings of the 9th ASCE Specialty Conference on Probabilistic Mechanics and Structural Reliability.
Wood, G.A., Kwok, K.C.S., Motteram, N.A., Fletcher, D.A., 2001. Physical and numerical modelling of thunderstorm downbursts. J. Wind Eng. Ind. Aerodyn. 89, 535–552.
Xu, Z., Hangan, H., 2008. Scale, boundary and inlet condition effects on impinging jets. J. Wind Eng. Ind. Aerodyn. 96, 2383–2402.
Zhang, Y., Hu, H., Sarkar, P.P., 2014. Comparison of microburst-wind loads on low-rise structures of various geometric shapes. J. Wind Eng. Ind. Aerodyn. 133, 181–190.
Zhang, Y., Sarkar, P., Hu, H., 2013. An experimental study of flow fields and wind loads on gable-roof building models in microburst-like wind. Exp. Fluids 54, 1–21.